iScience

CellPress

Article

Eomes partners with PU.1 and MITF to Regulate Transcription Factors Critical for osteoclast differentiation

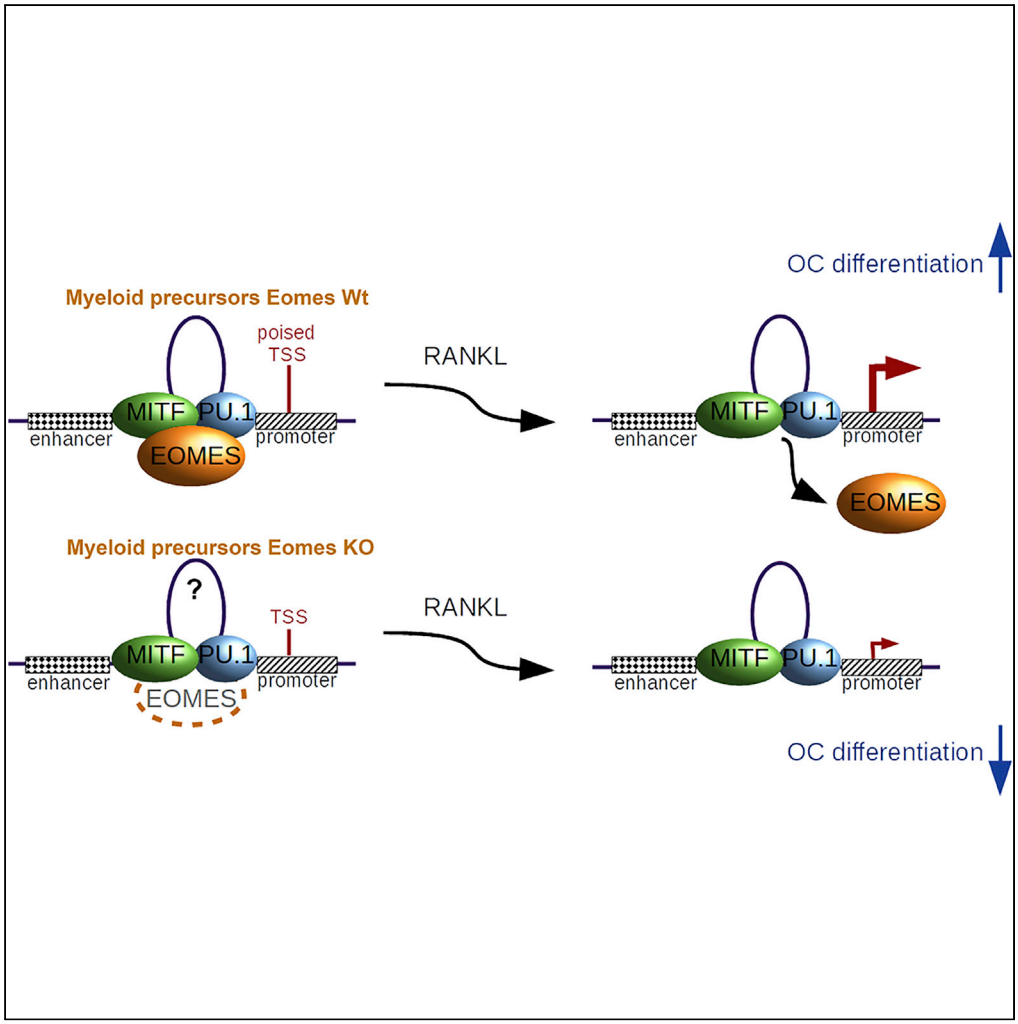

Heather A. Carey, Blake E. Hildreth III, Devadoss J. Samuvel, ..., Julia F. Charles, Michael C. Ostrowski, Sudarshana M. Sharma

ostrowsk@musc.edu (M.C.O.)
sharmas@musc.edu (S.M.S.)

HIGHLIGHTS

Genomics and systems biology approaches can decipher transcription factor interactions

Motif analysis of MITF and PU.1 ChIP-seq peaks identified EOMES as a cofactor

This is the first report of EOMES' function in the myeloid compartment

EOMES knockdown results in reduced osteoclast formation and function

Carey et al., iScience *11*, 238–245
January 25, 2019
https://doi.org/10.1016/j.isci.2018.12.018

iScience

CellPress

Article

Eomes partners with PU.1 and MITF to Regulate Transcription Factors Critical for osteoclast differentiation

Heather A. Carey,[1,6] Blake E. Hildreth III,[1,2,3,6] Devadoss J. Samuvel,[3] Katie A. Thies,[1,3] Thomas J. Rosol,[2,4] Ramiro E. Toribio,[2] Julia F. Charles,[5] Michael C. Ostrowski,[1,3,*] and Sudarshana M. Sharma[1,3,7,*]

SUMMARY

Bone-resorbing osteoclasts (OCs) are derived from myeloid precursors (MPs). Several transcription factors are implicated in OC differentiation and function; however, their hierarchical architecture and interplay are not well known. Analysis for enriched motifs in PU.1 and MITF chromatin immunoprecipitation coupled with high-throughput sequencing (ChIP-seq) data from differentiating OCs identified eomesodermin (EOMES) as a potential novel binding partner of PU.1 and MITF at genes critical for OC differentiation and function. We were able to demonstrate using co-immunoprecipitation and sequential ChIP analysis that PU.1, MITF, and EOMES are in the same complex and present as a complex at OC genomic loci. Furthermore, EOMES knockdown in MPs led to osteopetrosis associated with decreased OC differentiation and function both *in vitro* and *in vivo*. Although EOMES is associated with embryonic development and other hematopoietic lineages, this is the first study demonstrating the requirement of EOMES in the myeloid compartment.

INTRODUCTION

Hematopoiesis gives rise to a spectrum of cell types that are essential for normal immune and homeostatic functions throughout the body. Within this differentiation cascade, cells of the myeloid lineage give rise to bone-resorbing osteoclasts (OCs). In bones, OC differentiation from myeloid precursors (MPs) and subsequent OC function are regulated by microenvironmental cues from the surrounding stromal cells, in particular bone-forming osteoblasts. Downstream signaling through the CSF1/CSF1R and RANKL/RANK axes in the MPs, and later in the OCs, results in the activation of multiple signaling pathways and transcription factors (TFs) essential for OC differentiation, including PU.1, MITF, and NFATc1 (Hodgkinson et al., 1993; Takayanagi et al., 2002; Tondravi et al., 1997).

The ETS family member PU.1 is essential for myeloid lineage commitment (Iwasaki et al., 2005). We have shown that PU.1 and MITF physically and genetically interact to regulate a complex TF network regulating the course of OC differentiation, and ultimately OC function (Carey et al., 2018; Luchin et al., 2001; Sharma et al., 2007). Several of these PU.1-bound TF gene loci are present at the distal enhancer and "superenhancer" elements known to contain other TF-binding loci (Carey et al., 2018).

Eomesodermin (EOMES) was first identified as an essential developmental molecule controlling extraembryonic trophoblast formation (Ciruna and Rossant, 1999; Russ et al., 2000). EOMES has since been shown to be essential for (1) regulating mesoderm cell function and digit formation and (2) cerebral cortex development, patterning, and neurogenesis (Russ et al., 2000; Sessa et al., 2008; Sheeba and Logan, 2017). However, in postnatal life, EOMES has been predominately described along with the closely related T-box TF, T-bet, as a key regulator of $CD8^+$ T cell and natural killer (NK) cell maturation and function (Gordon et al., 2012; Intlekofer et al., 2005; Pearce et al., 2003).

In this study, we have demonstrated by motif-finding algorithms that the T-box TF EOMES is highly enriched in PU.1 and MITF co-bound peaks in MPs and OCs. Furthermore, EOMES physically interacts with PU.1 and MITF, co-binding these factors in a PU.1/MITF/EOMES complex at key OC-specific TF genomic loci, which we have previously shown to be bound by PU.1 and MITF (Carey et al., 2018). EOMES

[1]Department of Cancer Biology and Genetics and Comprehensive Cancer Center, The Ohio State University Wexner Medical Center, Columbus, OH 43210, USA

[2]College of Veterinary Medicine, The Ohio State University, Columbus, OH 43210, USA

[3]Department of Biochemistry and Molecular Biology and Hollings Cancer Center, Medical University of South Carolina, Hollings Cancer Center, 86 Jonathan Lucas St, Charleston, SC 29425, USA

[4]Department of Biomedical Sciences, Heritage College of Osteopathic Medicine, Ohio University, Athens, OH 45701, USA

[5]Department of Medicine, Division of Rheumatology, Immunology and Allergy, Brigham and Women's Hospital and Harvard Medical School, Boston, MA, USA

[6]These authors contributed equally

[7]Lead Contact

*Correspondence: ostrowsk@musc.edu (M.C.O.), sharmas@musc.edu (S.M.S.)

https://doi.org/10.1016/j.isci.2018.12.018

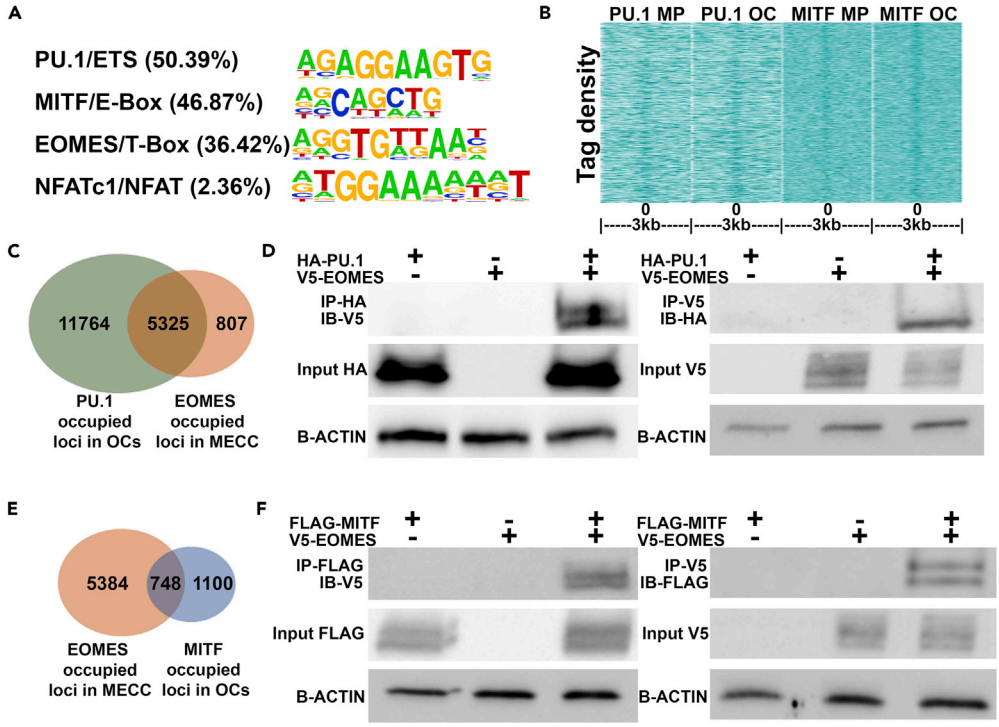

Figure 1. EOMES Interacts with PU.1 and MITF to Regulate OC-Determining Gene Loci

(A) Motifs enriched in MITF and PU.1 overlapped peaks in OCs with their percentage of occurrence.

(B) K means clustering diagram showing the density of PU.1 and MITF ChIP-seq fragments in MPs and OCs around EOMES-bound regions in murine embryonic cerebral cortex.

(C) Overlap of bound gene loci between EOMES ChIP-seq from MECC and PU.1 ChIP-seq in OCs.

(D) coIP experiments involving HA-PU.1 IP followed by V5-EOMES western blot in HEK293 cells overexpressing V5-tagged EOMES and HA-tagged PU.1 (left). Complementary experiments involving V5-EOMES immunoprecipitation (IP) followed by HA-PU.1 western blot in the same cells (right).

(E) Overlap of gene loci between EOMES ChIP-seq from MECC and MITF ChIP-seq in OCs.

(F) coIP experiments involving FLAG-MITF IP followed by V5-EOMES western blot in HEK293 cells overexpressing V5-tagged EOMES and FLAG-tagged MITF (left). Complementary experiments involving V5-EOMES IP followed by FLAG-MITF western blot in the same cells (right).

See also Figure S1.

knockdown in murine MPs leads to decreased OC differentiation and function *in vitro* and *in vivo*. Although EOMES is associated with other hematopoietic lineages, this is the first study demonstrating the requirement of EOMES in OC differentiation, where it is a novel co-partner of PU.1 and MITF.

RESULTS

EOMES Interacts with PU.1 and MITF to Regulate OC-Determining Gene Loci

We previously performed PU.1 and MITF chromatin immunoprecipitation coupled with high-throughput sequencing (ChIP-seq) in MPs and OCs. This revealed a conserved TF network regulating OC differentiation that is governed by PU.1 and MITF (Carey et al., 2018). To identify any novel binding partners that may also be important in establishing the OC TF network, we performed motif analysis of PU.1/MITF co-bound peaks in OCs. Apart from PU.1/ETS and MITF/E-Box motifs, a T-Box signature typical for EOMES/TBR2 was most enriched in PU.1/MITF co-bound peaks (Figure 1A). To evaluate the validity of these findings, we first analyzed a publicly available dataset of EOMES ChIP-seq from murine embryonic cerebral cortex (MECC) (Sessa et al., 2017). We evaluated the tag densities of both PU.1 and MITF in both MPs and OCs around EOMES-bound regions in MECC. These results indicated that the EOMES-occupied loci were associated with regions with higher PU.1 and MITF binding, as determined by K means clustering (Figure 1B). Furthermore, of the 17,089 genes associated with PU.1 binding in OCs, 31% of the genes were also associated with EOMES binding in MECC (Figure 1C). Tag densities of PU.1 occupancy from both MPs and OCs around MECC EOMES ChIP-seq peaks indicated that within 500 bp of EOMES peaks several PU.1 peaks may exist (Figure S1A).

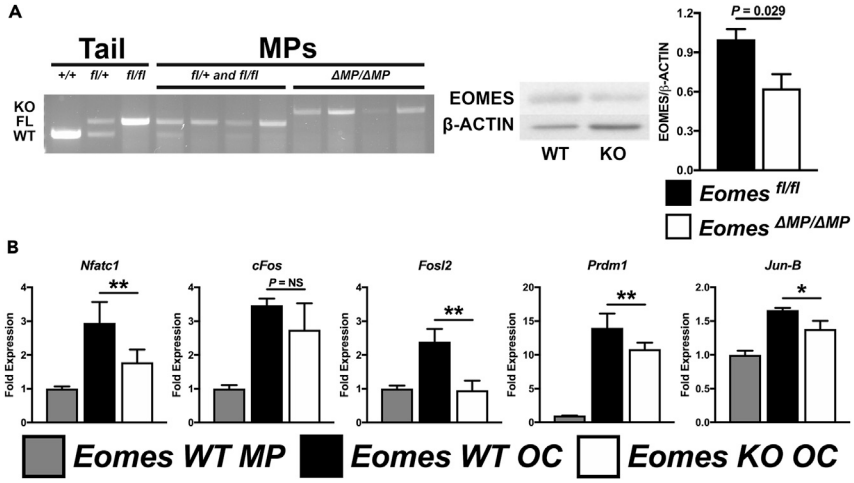

Figure 2. Myeloid-Specific Knockdown of *Eomes* Disrupts the Expression of OC-Specific TFs

(A) Knockdown of EOMES specifically in MPs (*Eomes*$^{\Delta MP/\Delta MP}$) was confirmed by (1) DNA genotyping PCR (with historical genomic tail-tip extracted DNA as reference) and (2) western blot analysis (with quantification, n = 2) following 3 days treatment with tamoxifen using myeloid-lineage-specific *Csf1rTAMCre* in combination with *Eomes*$^{fl/fl}$ mice when compared with *Eomes*$^{fl/fl}$, *Eomes*$^{fl/+}$, or *Eomes*$^{+/+}$ controls.

(B) Evaluation of key pro-osteoclastogenic TFs by quantitative real-time RT-PCR (n = 2–6). For all figures and subfigures, data are represented as mean ± SD for all bar graphs and all images are representative. *p < 0.05, **p < 0.01. KO, knockout; WT, wild-type.

See also Figure S2.

To examine whether PU.1 could physically interact with EOMES, we overexpressed V5-tagged EOMES with HA-tagged PU.1 in HEK293 cells followed by co-immunoprecipitation (coIP). Upon HA-PU.1 pull-down and probing for V5-EOMES by V5 antibody, an EOMES/PU.1 interaction was present (Figure 1D; left). In complementary experiments when EOMES complexes were pulled down with V5 antibody, a PU.1/EOMES interaction was also detected (Figure 1D; right). Next, we scrutinized whether MITF-occupied loci in OCs were also associated with EOMES-bound loci in MECC and found that 12% of the MITF-occupied sites overlapped with the EOMES-bound genes (Figure 1E), with the highest MITF tag density in MPs and OCs within 50 bases of EOMES peak centers in MECC (Figure S1B). FLAG-tagged MITF and V5-tagged EOMES overexpression in HEK293 cells followed by coIP also revealed an interaction between MITF and EOMES (Figure 1F).

Myeloid-Specific Knockdown of EOMES Disrupts the Expression of OC-Specific TFs

We have shown that the PU.1-MITF regulatory axis is a predominant regulator of the OC-specific TF network (Carey et al., 2018). To evaluate the molecular functions regulated by EOMES, we examined the molecular processes enriched in EOMES-associated genes from MECC using the ToppGene suite (Chen et al., 2009) and found that TF and promoter binding were highly enriched (Figure S2A). To verify if EOMES is essential for the expression of any of the TFs identified in the PU.1-MITF regulatory network, we used a tamoxifen-inducible, myeloid lineage-specific *Csf1rTAMCre* in combination with *Eomes*$^{fl/fl}$ mice to generate *Eomes*$^{\Delta MP/\Delta MP}$ mice with tamoxifen induction. EOMES knockdown in MPs was confirmed by both genotyping and western blot (Figure 2A). *Eomes*$^{\Delta MP/\Delta MP}$ mice showed a significant decrease in EOMES protein expression in MPs compared with controls (p = 0.029, Figure 2A). *In vitro* differentiation of MPs into OCs from *Eomes*$^{\Delta MP/\Delta MP}$ mice and control littermates revealed a significant reduction in the upregulation of pro-osteoclastogenic TFs, *Nfatc1*, *Fosl2*, *Prdm1*, and *Jun-B* when compared with controls (p < 0.05, Figure 2B). Although *cFos* upregulation in *Eomes*$^{\Delta MP/\Delta MP}$ OCs was reduced compared with controls, this did not reach statistical significance (p = 0.383, Figure 2B). In addition, TFs with known anti-osteoclastogenic effects, *Irf8* and *Bcl6*, trended to be significantly increased in OCs following EOMES deletion (p = 0.074 and 0.060, respectively, Figure S2B).

The PU.1-MITF-EOMES Complex Drives Nfatc1 Expression by Association with the Looping Peak within the Nfatc1 Superenhancer

We have recently identified a conserved intronic enhancer in the OC master regulator *Nfatc1* that requires PU.1 to loop back to the proximal promoter by means of changes in chromatin conformation (Carey et al., 2018).

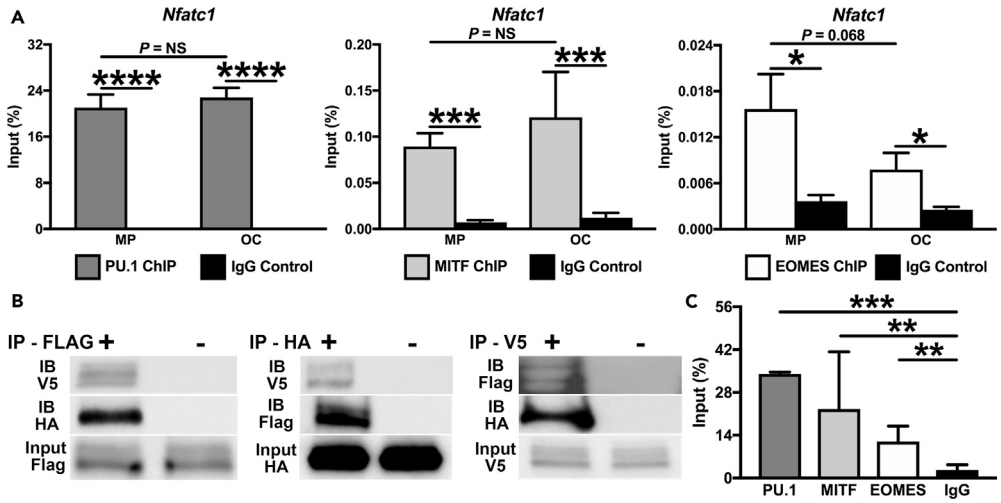

Figure 3. The PU.1-MITF-EOMES Complex Drives *Nfatc1* Expression by Association with the Looping Peak within the *Nfatc1* Superenhancer

(A) Conventional ChIP of PU.1, MITF, and EOMES binding at the conserved intronic enhancer of *Nfatc1* in MPs and OCs (n = 2–3).

(B) HA-PU.1, FLAG-MITF, or V5-EOMES immunoprecipitation (IP) followed by HA-PU.1, FLAG-MITF, or V5-EOMES western blot in HEK293 cells co-transfected with FLAG-MITF, HA-PU.1, and V5-EOMES.

(C) Sequential ChIP using PU.1, MITF, and EOMES antibodies following initial PU.1 ChIP in MPs (ReChIP) at the looping peak of *Nfatc1*. *p < 0.05, **p < 0.01, ***p < 0.001, ****p < 0.0001.

Thus we evaluated whether EOMES directly binds to this *Nfatc1* enhancer co-bound by PU.1 and MITF (Figure 3A). There was significant enrichment of PU.1, MITF, and EOMES at the *Nfatc1* enhancer in both MPs and OCs when compared with IgG controls ($p < 0.05$). Interestingly, whereas PU.1 and MITF occupancy is sustained at *Nfatc1* as MPs differentiated into OCs (Figure 3A), EOMES is present at a lower abundance in OCs when compared with MPs ($p = 0.068$, Figure 3A).

Next, we verified whether EOMES could represent a subunit of the PU.1-MITF complex by co-expression of FLAG-MITF, HA-PU.1, and V5-EOMES in HEK293 cells. In a series of complimentary experiments, when the total cell lysate was pulled down with (1) FLAG-MITF and probed for V5-EOMES and HA-PU.1 (left), (2) HA-PU.1 and probed for V5-EOMES and FLAG-MITF (middle), or (3) V5-EOMES and probed for FLAG-MITF and HA-PU.1 (right), all signals were detected in the immunoprecipitations (Figure 3B). These results indicated that PU.1, MITF, and EOMES all interact and can remain in a complex together. Previously, we have shown by ReChIP analysis that PU.1 and MITF can simultaneously occupy specific regions of chromatin (Hu et al., 2007). We again employed ReChIP to determine if EOMES can also interact with PU.1 and MITF while all occupy a regulatory site near the *Nfatc1* gene. For ReChIP, soluble chromatin from MPs was pulled down using the PU.1 antibody. After dissociation of the chromatin complex from the antibody, sequential ChIP was performed using PU.1, MITF, and EOMES antibodies. Using qRT-PCR with primers designed at the looping peak of *Nfatc1*, we observed that ~34% of the first immunoprecipitate (input for the second ChIP) was pulled down with the PU.1 antibody (Figure 3C). MITF was able to pull down ~23% of the first immunoprecipitate, and EOMES was able to pull down ~12%, all significantly more than the IgG control (~2.7%) ($p < 0.01$, Figure 3C). This result further indicates that PU.1, MITF, and EOMES can all interact in MPs and do so to regulate the expression of OC TF network genes like *Nfatc1*.

Myeloid-Specific EOMES Deletion Decreased OC Differentiation and Function *In Vivo* and *In Vitro*

$Eomes^{\Delta MP/\Delta MP}$ mice possessed increased bone mass when compared with control $Eomes^{fl/fl}$ mice upon micro-computed tomographic analysis (Figure 4A). Most notably, there was a significant increase in bone volume/total volume in the distal femoral metaphysis ($p = 0.013$) and cortical thickness in both the distal femoral metaphysis ($p = 0.038$) and diaphysis ($p = 0.016$) (Figure 4B). In addition, $Eomes^{\Delta MP/\Delta MP}$ mice displayed a significant increase in cumulative bone mineral density (BMD) ($p = 0.009$) and trabecular

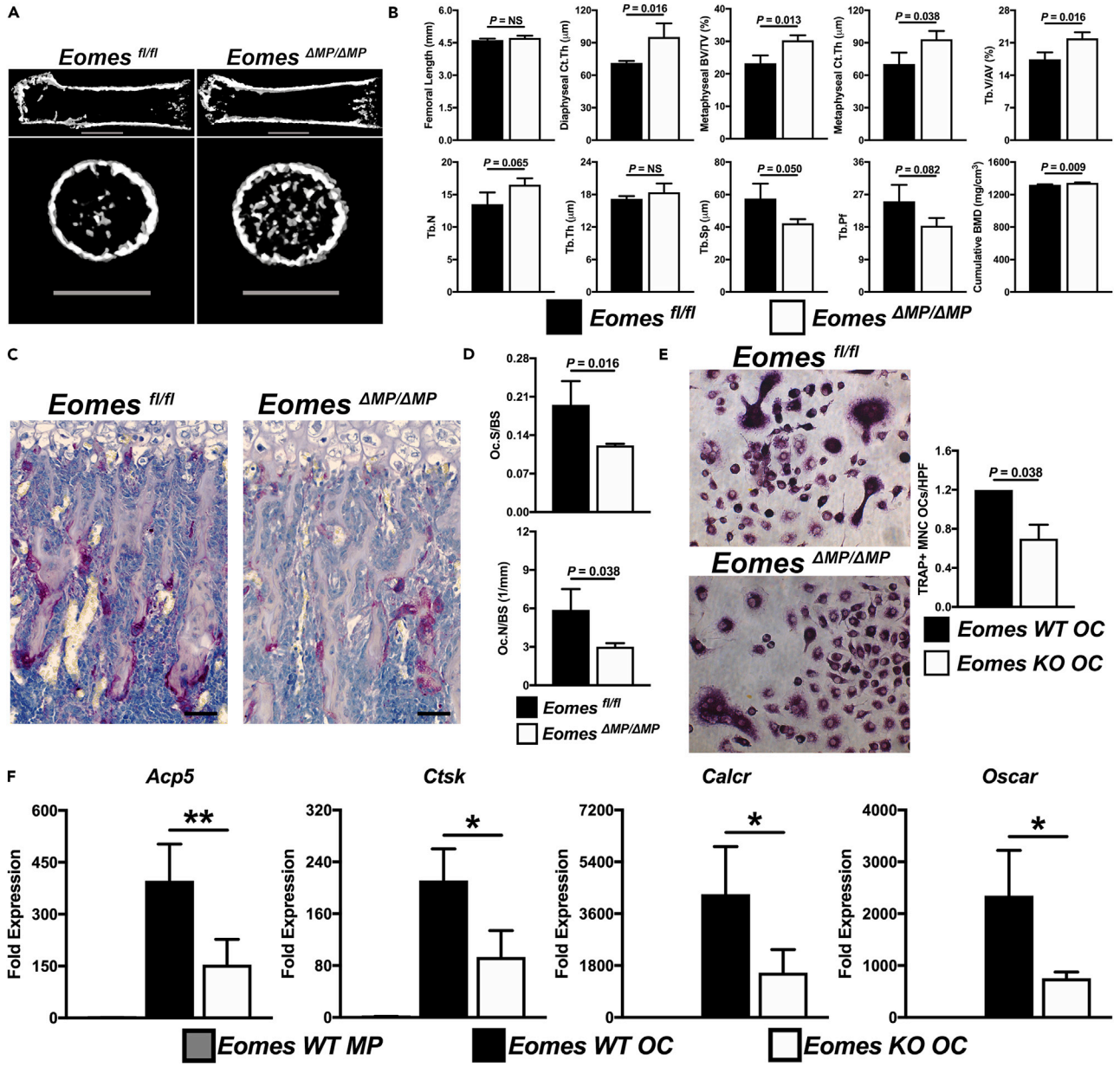

Figure 4. Myeloid-Specific *Eomes* Deletion Decreased OC Differentiation and Function *In Vivo* and *In Vitro*

(A) Femoral micro-computed tomographic (μCT) cross-sectional images in the craniocaudal view and the distal femoral metaphysis in the proximodistal view from 8-day-old $Eomes^{\Delta MP/\Delta MP}$ mice and $Eomes^{fl/fl}$ controls. Scale bars, 1 mm.

(B) μCT quantification of bone morphometric variables (n = 3). BMD, bone mineral density; BV/TV, bone volume/total volume; Ct.Th, cortical thickness; Tb.V/AV, trabecular volume/all bone volume; Tb.N, trabecular number; Tb.Sp, trabecular spacing; Tb.Pf, trabecular pattern factor; Tb.Th, trabecular thickness.

(C) Tartrate-resistant acid phosphatase (TRAP) staining (in violet) with hematoxylin counterstain to identify OCs in the distal femoral metaphysis of mice in (A). Scale bars, 50 μm.

(D) Histomorphometric quantification of Oc.S/BS and Oc.N/BS from (C) (n = 3). Oc.N/BS, OC number per bone surface; Oc.S/BS, OC surface per bone surface.

(E and F) (E) Representative images of *in vitro* TRAP-positive multinucleated OC formation from $Csf1rTAMCre;Eomes^{fl/fl}$ and $Eomes^{fl/fl}$ mice and quantification per high-powered field (HPF) (n = 2). (F) RT-PCR analysis of genes regulating OC differentiation and function in $Eomes^{fl/fl}$ (WT) MPs and OCs and $Eomes^{\Delta MP/\Delta MP}$ (*Eomes KO*) OCs after differentiation (n = 2–6). *p < 0.05, **p < 0.01. KO, knockout; WT, wild-type.

volume/all bone volume (p = 0.016), a trend toward a significant increase in trabecular number (p = 0.065), and a decrease in trabecular spacing (p = 0.050, Figure 4B). The statistical trend and decrease in trabecular pattern factor (p = 0.082) in $Eomes^{\Delta MP/\Delta MP}$ mice indicates greater trabecular connectivity (Figure 4B).

Based on our MP-specific deletion of EOMES, these results suggest that decreased osteoclastic bone resorption is responsible for the bone phenotype observed in *Eomes*$^{\Delta MP/\Delta MP}$ mice. In further support of this hypothesis, histomorphometric analysis revealed a significant reduction in both OC number ($p = 0.038$) and OC surface ($p = 0.016$) per bone surface in *Eomes*$^{\Delta MP/\Delta MP}$ mice compared with controls (Figures 4C and 4D). *In vitro* differentiation of OCs derived from *Eomes*$^{\Delta MP/\Delta MP}$ mice showed a significant reduction in the formation of TRAP-positive multinucleated OCs ($p = 0.038$, Figures 4E and 4A) and significant decrease in the expression of the OC marker genes *Acp5, Ctsk, Calcr,* and *Oscar* ($p < 0.05$, Figure 4F).

DISCUSSION

EOMES is the earliest expressed T-box gene during development (Ciruna and Rossant, 1999). Constitutive or conditional EOMES deletion has demonstrated its crucial role in lineage commitment, differentiation, and maintenance of multiple stem and progenitor cell populations (Pimeisl et al., 2013). The functionality of EOMES in post-natal life is best described in the context of the immune system, where it is a key regulator of cell-mediated immunity and T cell function (Intlekofer et al., 2005; Pearce et al., 2003). Here, the essential role of EOMES is evident in that it is a disease susceptibility loci for multiple diseases linked with T cell dysfunction (Berndt et al., 2016; Kim et al., 2015).

One of the key insights obtained in our study is the discovery that EOMES is a functional partner of PU.1 and MITF in regulating the TF network governing OC differentiation. Although EOMES is capable of inducing the full array of mesodermal cell types and genes (Sheeba and Logan, 2017), expression and functionality of EOMES in bone-resorbing OCs, or any cell of the myeloid lineage for that matter, has not been reported. Our results confirm that like the master myeloid regulator PU.1 (Carey et al., 2018), EOMES modulates OC differentiation by promoting the expression of pro-osteoclastogenic TFs and inhibiting the expression of TFs that negatively regulate OC differentiation, albeit to a lesser magnitude than PU.1. Our *in silico* analysis indicated high enrichment of the EOMES-binding motif in PU.1-MITF co-bound loci. Furthermore, when PU.1 and MITF tag densities were mapped against EOMES ChIP-seq peaks from MECC (Sessa et al., 2017), both PU.1 and MITF tags were enriched within 50 bp of the EOMES peak centers.

Our *in silico* results led us to query whether EOMES could interact with PU.1, MITF, or both. No physical interaction between EOMES and either MITF or ETS family TFs, like PU.1, has been previously reported. However, previous work has shown that EOMES regulates the expression of genes regulated by (1) MITF, such as granzyme B and interferon-γ, and (2) ETS1 and MEF (ETS family members), including perforin in certain lymphoid cell populations (Glimcher et al., 2004). Interestingly, in $CD8^+$ T cells, different chromatin conformations are associated with ETS family member and EOMES binding (Moskowitz et al., 2017). In the naive cell state, there is increased accessibility by ETS members, and in the memory cell state, an open conformation allows more ready access by EOMES (Moskowitz et al., 2017). In our study, we were able to demonstrate in the myeloid compartment that the ETS family TF, PU.1, and MITF, are in a complex with EOMES, which is found at the looping peak of the *Nfatc1* enhancer. These results indicate that in the looping peak of *Nfatc1*, EOMES associates with the PU.1-MITF complex in at least a subset of MPs. Considering that only a subset of MPs differentiate to form OCs *in vivo*, EOMES might be more specifically present only in those MPs committing to the OC precursor population. Previous work has shown that EOMES changes its binding profile during transition from one cell type to another, suggesting that its function may change at different points of differentiation (Tsankov et al., 2015). Conventional ChIP revealed that like PU.1 and MITF, EOMES is recruited and bound to a key TF locus essential for OC differentiation. Interestingly, we detected a statistical trend toward a lower abundance of EOMES binding on *Nfatc1* in OCs when compared with MPs. This suggests that EOMES is more essential in establishing chromatin dynamics in MPs than in differentiating OCs.

We demonstrated that MP-specific EOMES deletion disrupted the PU.1-MITF TF network and resulted in osteopetrosis *in vivo*, a finding consistent with decreased OC differentiation and function. Historically, EOMES knockout mice arrest at the blastocyst stage, resulting in early embryonic lethality (Russ et al., 2000). Lineage-specific EOMES deletion within the hematopoietic hierarchy using *Vav-Cre* has been reported (Gordon et al., 2012). However, whereas there was a global reduction in NK cells, which are of lymphoid origin, no investigation on changes within the myeloid lineage were reported (Gordon et al., 2012).

In summary, the work presented here is the first evidence of EOMES having a functional role in any cell of the myeloid lineage, where EOMES is a novel binding partner of PU.1 and MITF and works in conjunction with these factors to regulate the OC TF network.

Limitations of the Study

Although the systems biology approaches we used to identify EOMES as a partner of PU.1 and MITF are robust, they also give rise to several other "hits" due to the vast number of ETS DNA-binding domains. We filtered most of the ETS motifs as a subset of binding regions associated with PU.1, which is an ETS factor. An additional limitation is that due to the lack of reagents, the temporal kinetics of PU.1, MITF, and EOMES recruitment to target loci was not established in the current study.

METHODS

All methods can be found in the accompanying Transparent Methods supplemental file.

DATA AND SOFTWARE AVAILABILITY

Raw images of immunoprecipitation and western blot data used in this has been deposited to Mendeley depository and can be accessed at URL:http://dx.doi.org/10.17632/wdv72kxgjg.1.

SUPPLEMENTAL INFORMATION

Supplemental Information includes Transparent Methods and two figures and can be found with this article online at https://doi.org/10.1016/j.isci.2018.12.018.

ACKNOWLEDGMENTS

The authors are grateful to the core facilities involved in this work, OSU ULAR and MUSC DLAR, for animal care and Jason Bice of the OSU-CCC Solid Tumor Biology Histology Core for tissue preparation. Authors are grateful to Dr. Lyudmyla I. Sharma for the conceptualization and creation of graphical abstract. This work was supported by NIH-NIAMS Grant 2R01AR044719-15A (M.C.O. and S.S.M.).

AUTHOR CONTRIBUTIONS

Conceptualization, M.C.O., and S.M.S.; Methodology, H.A.C., J.F.C., M.C.O., and S.M.S; Investigation, H.A.C., B.E.H., D.J.S., K.A.T., and S.M.S; Formal Analysis, B.E.H., T.J.R., R.E.T., J.F.C., and S.M.S; Visualization, B.E.H., D.J.S., and S.M.S; Writing – Original Draft, H.A.C., B.E.H., and S.M.S; Writing – Review & Editing, B.E.H., M.C.O., J.F.C., and S.M.S.; Funding Acquisition, M.C.O. and S.M.S.; Resources, M.C.O., J.F.C., R.E.T., and S.M.S.; Supervision, M.C.O. and S.M.S.

DECLARATION OF INTERESTS

The authors declare no competing interests.

Received: September 21, 2018
Revised: December 12, 2018
Accepted: December 20, 2018
Published: January 25, 2019

REFERENCES

Berndt, S.I., Camp, N.J., Skibola, C.F., Vijai, J., Wang, Z., Gu, J., Nieters, A., Kelly, R.S., Smedby, K.E., Monnereau, A., et al. (2016). Meta-analysis of genome-wide association studies discovers multiple loci for chronic lymphocytic leukemia. Nat. Commun. *7*, 10933.

Carey, H.A., Hildreth, B.E., 3rd, Geisler, J.A., Nickel, M.C., Cabrera, J., Ghosh, S., Jiang, Y., Yan, J., Lee, J., Makam, S., et al. (2018). Enhancer variants reveal a conserved transcription factor network governed by PU.1 during osteoclast differentiation. Bone Res. *6*, 8.

Chen, J., Bardes, E.E., Aronow, B.J., and Jegga, A.G. (2009). ToppGene Suite for gene list enrichment analysis and candidate gene prioritization. Nucleic Acids Res. *37*, W305–W311.

Ciruna, B.G., and Rossant, J. (1999). Expression of the T-box gene Eomesodermin during early mouse development. Mech. Dev. *81*, 199–203.

Glimcher, L.H., Townsend, M.J., Sullivan, B.M., and Lord, G.M. (2004). Recent developments in the transcriptional regulation of cytolytic effector cells. Nat. Rev. Immunol. *4*, 900–911.

Gordon, S.M., Chaix, J., Rupp, L.J., Wu, J., Madera, S., Sun, J.C., Lindsten, T., and Reiner, S.L. (2012). The transcription factors T-bet and Eomes control key checkpoints of natural killer cell maturation. Immunity *36*, 55–67.

Hodgkinson, C.A., Moore, K.J., Nakayama, A., Steingrimsson, E., Copeland, N.G., Jenkins, N.A., and Arnheiter, H. (1993). Mutations at the mouse microphthalmia locus are associated with defects in a gene encoding a novel basic-helix-loop-helix-zipper protein. Cell *74*, 395–404.

Hu, R., Sharma, S.M., Bronisz, A., Srinivasan, R., Sankar, U., and Ostrowski, M.C. (2007). Eos, MITF, and PU.1 recruit corepressors to osteoclast-specific genes in committed myeloid progenitors. Mol. Cell. Biol. *27*, 4018–4027.

Intlekofer, A.M., Takemoto, N., Wherry, E.J., Longworth, S.A., Northrup, J.T., Palanivel, V.R., Mullen, A.C., Gasink, C.R., Kaech, S.M., Miller, J.D., et al. (2005). Effector and memory CD8+ T cell fate coupled by T-bet and eomesodermin. Nat. Immunol. *6*, 1236–1244.

Iwasaki, H., Somoza, C., Shigematsu, H., Duprez, E.A., Iwasaki-Arai, J., Mizuno, S., Arinobu, Y., Geary, K., Zhang, P., Dayaram, T., et al. (2005).

Distinctive and indispensable roles of PU.1 in maintenance of hematopoietic stem cells and their differentiation. Blood *106*, 1590–1600.

Kim, K., Bang, S.Y., Lee, H.S., Cho, S.K., Choi, C.B., Sung, Y.K., Kim, T.H., Jun, J.B., Yoo, D.H., Kang, Y.M., et al. (2015). High-density genotyping of immune loci in Koreans and Europeans identifies eight new rheumatoid arthritis risk loci. Ann. Rheum. Dis. *74*, e13.

Luchin, A., Suchting, S., Merson, T., Rosol, T.J., Hume, D.A., Cassady, A.I., and Ostrowski, M.C. (2001). Genetic and physical interactions between Microphthalmia transcription factor and PU.1 are necessary for osteoclast gene expression and differentiation. J. Biol. Chem. *276*, 36703–36710.

Moskowitz, D.M., Zhang, D.W., Hu, B., Le Saux, S., Yanes, R.E., Ye, Z., Buenrostro, J.D., Weyand, C.M., Greenleaf, W.J., and Goronzy, J.J. (2017). Epigenomics of human CD8 T cell differentiation and aging. Sci. Immunol. *2*, 1–13.

Pearce, E.L., Mullen, A.C., Martins, G.A., Krawczyk, C.M., Hutchins, A.S., Zediak, V.P., Banica, M., DiCioccio, C.B., Gross, D.A., Mao, C.A., et al. (2003). Control of effector CD8+ T cell function by the transcription factor Eomesodermin. Science *302*, 1041–1043.

Pimeisl, I.M., Tanriver, Y., Daza, R.A., Vauti, F., Hevner, R.F., Arnold, H.H., and Arnold, S.J. (2013). Generation and characterization of a tamoxifen-inducible Eomes(CreER) mouse line. Genesis *51*, 725–733.

Russ, A.P., Wattler, S., Colledge, W.H., Aparicio, S.A., Carlton, M.B., Pearce, J.J., Barton, S.C., Surani, M.A., Ryan, K., Nehls, M.C., et al. (2000). Eomesodermin is required for mouse trophoblast development and mesoderm formation. Nature *404*, 95–99.

Sessa, A., Ciabatti, E., Drechsel, D., Massimino, L., Colasante, G., Giannelli, S., Satoh, T., Akira, S., Guillemot, F., and Broccoli, V. (2017). The Tbr2 molecular network controls cortical neuronal differentiation through complementary genetic and epigenetic pathways. Cereb. Cortex *27*, 3378–3396.

Sessa, A., Mao, C.A., Hadjantonakis, A.K., Klein, W.H., and Broccoli, V. (2008). Tbr2 directs conversion of radial glia into basal precursors and guides neuronal amplification by indirect neurogenesis in the developing neocortex. Neuron *60*, 56–69.

Sharma, S.M., Bronisz, A., Hu, R., Patel, K., Mansky, K.C., Sif, S., and Ostrowski, M.C. (2007). MITF and PU.1 recruit p38 MAPK and NFATc1 to target genes during osteoclast differentiation. J. Biol. Chem. *282*, 15921–15929.

Sheeba, C.J., and Logan, M.P. (2017). The roles of T-box genes in vertebrate limb development. Curr. Top. Dev. Biol. *122*, 355–381.

Takayanagi, H., Kim, S., Koga, T., Nishina, H., Isshiki, M., Yoshida, H., Saiura, A., Isobe, M., Yokochi, T., Inoue, J., et al. (2002). Induction and activation of the transcription factor NFATc1 (NFAT2) integrate RANKL signaling in terminal differentiation of osteoclasts. Dev. Cell *3*, 889–901.

Tondravi, M.M., McKercher, S.R., Anderson, K., Erdmann, J.M., Quiroz, M., Maki, R., and Teitelbaum, S.L. (1997). Osteopetrosis in mice lacking haematopoietic transcription factor PU.1. Nature *386*, 81–84.

Tsankov, A.M., Gu, H., Akopian, V., Ziller, M.J., Donaghey, J., Amit, I., Gnirke, A., and Meissner, A. (2015). Transcription factor binding dynamics during human ES cell differentiation. Nature *518*, 344–349.

ISCI, Volume *11*

Supplemental Information

Eomes partners with PU.1 and MITF to Regulate Transcription Factors Critical for osteoclast differentiation

Heather A. Carey, Blake E. Hildreth III, Devadoss J. Samuvel, Katie A. Thies, Thomas J. Rosol, Ramiro E. Toribio, Julia F. Charles, Michael C. Ostrowski, and Sudarshana M. Sharma

Eomes_Suppl_Fig1

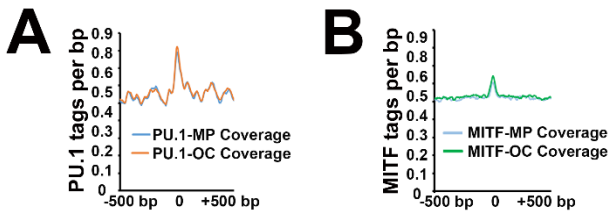

Supplemental Figure 1, Related to Figure 1: A) Tag densities of PU.1 occupancy from both MPs and OCs around MECC EOMES ChIP-Seq peaks. B) Tag densities of MITF occupancy from both MPs and OCs around MECC EOMES ChIP-Seq peaks. For both A) and B), 0 on the X axis indicates the EOMES peak center.

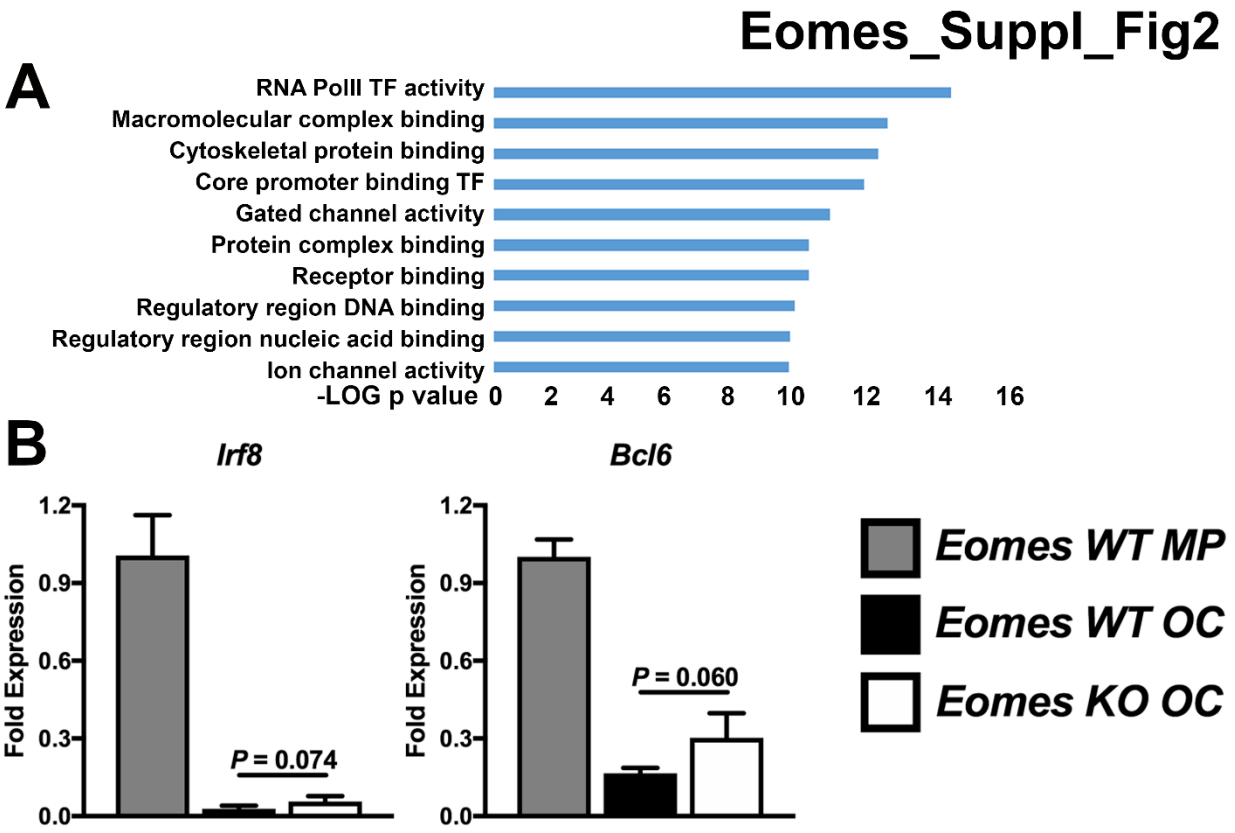

Supplemental Figure 2, Related to Figure 2: A) ToppGene enrichment of EOMES-associated genes to evaluate the molecular functions regulated by EOMES. B) Evaluation of key anti-osteoclastogenic TFs by quantitative real-time RT-PCR (n=2-4).

Transparent Methods

Cell culture and transfection

Cells were grown in complete medium – DMEM (high glucose) with 10% FBS, 2 mM L-glutamine, and 50 U/ml penicillin/streptomycin (Invitrogen). For transient transfections, $2x10^5$ HEK-293 cells were transfected with 2 µg of plasmid using Lipofectamine® 3000 (Invitrogen). The following plasmids were used – FLAG-MITF, HA-PU.1, V5-EOMES, and control V5-His.

Genomic analysis

An external dataset for EOMES ChIP-seq (Sessa et al., 2017) was aligned to the mouse genome *mm9* using Bowtie2 software (Langmead et al., 2009). Peak calling and motif analysis were performed with HOMER software (Heinz et al., 2010). Centered K means clustering was done using Cluster 3.0 and visualized using the Java-Treeview program (de Hoon et al., 2004).

Animals

All use was approved by the Ohio State University and Medical University of South Carolina IACUCs (Protocols: 2007A0120-R2, 2016A00000035, and IACUC-2017-00064). Mice were on a C57BL/6J background (F10 or further). C57BL/6J wild type and *Eomes*$^{fl/fl}$ mice were purchased from Jackson Laboratories. Mice possessing either tamoxifen-inducible or constitutively active myeloid lineage-specific *Csf1r* promoter driven *Cre* ((*Csf1rTAMCre* and *Csf1rCre*, respectively) were from Dr. Jeffrey Pollard (Albert Einstein College of Medicine) (Deng et al., 2010; Qian et al., 2011). Tamoxifen (Sigma-Aldrich) was dissolved in corn oil with 5% ethanol. For inducible myeloid-specific *Eomes* deletion (*Eomes*$^{\Delta MP/\Delta MP}$), *Csf1rTAMCre+;Eomes*$^{fl/fl}$ and *Eomes*$^{fl/fl}$ control littermate mice were injected I.P. with 50 µg tamoxifen/mouse/day on days 1, 2, and 3 after birth (Figure 2A). Since only neonatal mice were used in this study, both male and female mice were used concurrently.

Immunoprecipitation and Western blot

For IP experiments, different combinations of FLAG-MITF, HA-PU.1, and V5-EOMES were transfected into HEK-293 cells. Preparation of cell lysates, IP, and Western blot analysis were as previously described (Carey et al., 2016). Briefly, 200 µg of protein was incubated with **1)** anti-FLAG (Sigma-Aldrich Cat #1804); **2)** anti-HA (Cell Signaling Cat #3724); or **3)** anti-V5 (Sigma-Aldrich Cat #V8012) antibody overnight at 4°C while shaken. Immunoprecipitated proteins were recovered, washed in lysis buffer, and immunocomplexes released with 2X SDS sample buffer.

In vitro OC differentiation and TRAP staining

Mice with MP-specific deletion of *Eomes* (*Eomes*$^{\Delta MP/\Delta MP}$) using constitutive *Csf1rCre* and *Eomes*$^{fl/fl}$ control littermate mice were used. For confirmation of EOMES knockdown in MPs from *Eomes*$^{\Delta MP/\Delta MP}$ mice, genotyping PCR and confirmatory Western blot (described above) using rabbit anti-mouse EOMES primary antibody (Cell Signaling Technology Cat #4540) was performed after combined protein and DNA extraction using TRIzol (Invitrogen). Digested spleens or bone marrow flushes were enriched for MPs and differentiated into OCs for three days as previously described for gene expression analysis (Carey et al., 2018). To evaluate *in vitro* OC differentiation by the formation of TRAP-positive multinucleated OCs, mice with MP-specific deletion of *Eomes* (*Eomes*$^{\Delta MP/\Delta MP}$) using tamoxifen-inducible *Csf1rTAMCre* were used. *Csf1rTAMCre+;Eomes*$^{fl/fl}$ and *Eomes*$^{fl/fl}$ control littermate mice were injected I.P. with 50 µg tamoxifen/mouse/day on days 1, 2, and 3 after birth. Mice were harvested at eight days of age and bone marrow flushes enriched for MPs and differentiated into OCs for five days with tamoxifen in the medium. Cells were stained for TRAP using a Leukocyte Acid Phosphatase kit (Sigma-Aldrich). OCs were defined as TRAP-positive cells having three or more visible nuclei.

RT-qPCR

Total RNA isolation, cDNA synthesis, qPCR using Taqman Master Mix and Universal Probe Library probes and primers (Roche), and data analysis was performed as previously described (Carey et al., 2018).

ChIP and Re-ChIP

Rabbit anti-mouse PU.1 and MITF antibodies used for ChIP have been described previously (Sharma et al., 2007). The same rabbit anti-mouse EOMES antibody used for Western blot was also used. ChIP and Re-ChIP were performed as previously described (Sharma et al., 2007).

μCT and bone morphometry

For myeloid-specific *Eomes* deletion (*Eomes*$^{\Delta MP/\Delta MP}$), inducible *Csf1rTAMCre+;Eomes*$^{fl/fl}$ and *Eomes*$^{fl/fl}$ control littermate mice were used. Femurs were dissected at 8 days of age, formalin-fixed for 24 hours, and maintained in 70% ethanol. μCT analysis was performed on an Inveon Preclinical CT scanner (Siemens AG) with a 9.7 μm resolution. The diaphyseal volume of interest (VOI) was defined as the central 5% and the distal metaphyseal VOI was 2.5% of the femoral length.Bones were analyzed using 3D bone morphometry analysis software from the μCT scanner manufacturer. Segmentation thresholds were constant and VOIs analyzed in a blinded manner.

In vivo TRAP staining and histomorphometry

Femurs from *Eomes*$^{\Delta MP/\Delta MP}$ and *Eomes*$^{fl/fl}$ control mice used for μCT were decalcified in 14% EDTA for 2 weeks, embedded in paraffin, and cut to 4 μm thick sagittal sections. Sections were stained for TRAP (Sigma-Aldrich) and counterstained with hematoxylin. OCs were defined as TRAP positive cells having three or more visible nuclei. Slides were scanned (Aperio

ScanScope XT) and OC number and surface and trabecular surface measured to calculate Oc.S/BS and Oc.N/BS (Aperio ImageScope software).

Statistical analysis

Data are expressed as mean ± 1 standard deviation. Non-normally distributed data and/or data with unequal variance underwent inverse transformation. Comparisons were then performed between **1)** two groups with an unpaired t-test and **2)** three or more groups with a one-way ANOVA and Holm-Sidak post-hoc analysis (normal distribution and equal variance). Quantified EOMES Western blot protein levels were compared between controls and $Eomes^{\Delta MP/\Delta MP}$ mice with a one-tailed t-test. ReChIP comparisons were done using a one-way ANOVA and Holm-Sidak post-hoc analysis with IgG as the control group. Gene expression and ChIP comparisons were performed with ΔCt values. Statistical analyses were conducted with Prism 7 (GraphPad Software) with a statistical significance of $P < 0.05$.

Data and Software Availability

Raw images of immunoprecipitation and western blot data used in this has been deposited to Mendeley depository and can be accessed at URL: http://dx.doi.org/10.17632/wdv72kxgjg.1

Supplemntary References

Carey, H.A., Bronisz, A., Cabrera, J., Hildreth, B.E., 3rd, Cuitino, M., Fu, Q., Ahmad, A., Toribio, R.E., Ostrowski, M.C., and Sharma, S.M. (2016). Failure to Target RANKL Signaling Through p38-MAPK Results in Defective Osteoclastogenesis in the Microphthalmia Cloudy-Eyed Mutant. J Cell Physiol *231*, 630-640.
Carey, H.A., Hildreth, B.E., 3rd, Geisler, J.A., Nickel, M.C., Cabrera, J., Ghosh, S., Jiang, Y., Yan, J., Lee, J., Makam, S*., et al.* (2018). Enhancer variants reveal a conserved transcription factor network governed by PU.1 during osteoclast differentiation. Bone Res *6*, 8.
de Hoon, M.J., Imoto, S., Nolan, J., and Miyano, S. (2004). Open source clustering software. Bioinformatics *20*, 1453-1454.
Deng, L., Zhou, J.F., Sellers, R.S., Li, J.F., Nguyen, A.V., Wang, Y., Orlofsky, A., Liu, Q., Hume, D.A., Pollard, J.W*., et al.* (2010). A novel mouse model of inflammatory bowel disease links mammalian target of rapamycin-dependent hyperproliferation of colonic epithelium to inflammation-associated tumorigenesis. Am J Pathol *176*, 952-967.
Heinz, S., Benner, C., Spann, N., Bertolino, E., Lin, Y.C., Laslo, P., Cheng, J.X., Murre, C., Singh, H., and Glass, C.K. (2010). Simple combinations of lineage-determining transcription factors prime cis-regulatory elements required for macrophage and B cell identities. Mol Cell *38*, 576-589.
Langmead, B., Trapnell, C., Pop, M., and Salzberg, S.L. (2009). Ultrafast and memory-efficient alignment of short DNA sequences to the human genome. Genome Biol *10*, R25.
Qian, B.Z., Li, J., Zhang, H., Kitamura, T., Zhang, J., Campion, L.R., Kaiser, E.A., Snyder, L.A., and Pollard, J.W. (2011). CCL2 recruits inflammatory monocytes to facilitate breast-tumour metastasis. Nature *475*, 222-225.
Sessa, A., Ciabatti, E., Drechsel, D., Massimino, L., Colasante, G., Giannelli, S., Satoh, T., Akira, S., Guillemot, F., and Broccoli, V. (2017). The Tbr2 Molecular Network Controls Cortical Neuronal Differentiation Through Complementary Genetic and Epigenetic Pathways. Cereb Cortex *27*, 3378-3396.
Sharma, S.M., Bronisz, A., Hu, R., Patel, K., Mansky, K.C., Sif, S., and Ostrowski, M.C. (2007). MITF and PU.1 recruit p38 MAPK and NFATc1 to target genes during osteoclast differentiation. J Biol Chem *282*, 15921-15929.